Electron momentum density of hexagonal Zn studied by high-resolution Compton scattering

Marek Brancewicz,[a]* Andrzej Andrejczuk,[a] Eugeniusz Żukowski,[a] Ludwik Dobrzyński,[b] Yoshiharu Sakurai,[c] Masayoshi Itou[c] and Maciej Pylak[d]

[a]Faculty of Physics, University of Białystok, ul. Ciołkowskiego 1L, Białystok 15-245, Poland, [b]National Centre for Nuclear Research, ul. Andrzeja Sołtana 7, Otwock, Świerk 05-400, Poland, [c]Japan Synchrotron Radiation Research Institute (JASRI), 1-1-1 Kouto, Sayo-cho, Sayo-gun, Hyogo 679-5198, Japan, and [d]National Centre for Nuclear Research, ul. Pasteura 7, Warsaw 02-093, Poland. *Correspondence e-mail: m.brancewicz@uwb.edu.pl

High-resolution (0.12 a.u.) electron momentum density projections (Compton profiles) of a hexagonal Zn single crystal have been measured along five high-symmetry directions in reciprocal space. The experiment was performed with the use of 115.6 keV synchrotron radiation on the BL08W station at SPring-8. The quality of the measured Compton profiles is significantly better than that of previous medium- and high-resolution data. The experimental data were compared with the corresponding theoretical Korringa–Kohn–Rostoker (KKR) and density functional theory (DFT) calculations. Some minor and major differences between the two theoretical band-structure calculations have been observed. However, the good quality experimental results indicate their better agreement with DFT.

1. Introduction

The electronic structure of Zn ([Ar] $3d^{10}4s^2$) and other divalent hexagonal close-packed (hcp) transition metals like Mg ([Ne] $3s^2$) and Cd ([Kr] $4d^{10}5s^2$) have been the subject of experimental (Joseph & Gordon, 1962; Steenhaut & Goodrich, 1970; Almond *et al.*, 1975; Perkkiö *et al.*, 1991; Reniewicz *et al.*, 2001; Bellin *et al.*, 2004; Brancewicz *et al.*, 2007) and theoretical (Harrison, 1962; Stark & Falicov, 1967; Borghese & Denti, 1971, 1974; Daniuk *et al.*, 1989; Novikov *et al.*, 1999) studies for many years. Experimental data concerned with the electronic structure of these relatively simple metals, where crystal symmetry mainly determines the behaviour of the conduction electrons, are of relevance to *ab initio* band-structure calculations. Therefore these metals are a great test field for the most fundamental concepts and approximations of one-electron band theories.

Compton scattering is the most direct and well established experimental method to test electronic structures in condensed matter physics. The measured Compton profile (CP), $J(p_z)$, is a one-dimensional projection (the so-called directional CP in the case of single crystals) of the 3D electron momentum density distribution $n(\mathbf{p})$ (Cooper *et al.*, 2004) and, within the limits of the impulse approximation, is directly connected to the many-body ground-state electronic wavefunctions approximated by the set of calculated electronic single-particle wavefunctions $\psi_j(\mathbf{r})$:

$$J(p_z) = \int_{-\infty}^{\infty} \int_{-\infty}^{\infty} n(\mathbf{p}) \, dp_x \, dp_y, \qquad (1)$$

where
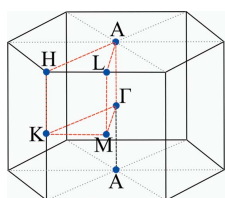
|ΓA|=0.336 a.u.
|ΓM|=0.721 a.u.
|ΓL|=0.796 a.u.
|ΓK|=0.833 a.u.
|ΓH|=0.898 a.u.

Table 1
Characteristics of the Zn samples and some experimental details.

Direction in reciprocal space	Direction in first BZ	Sample dimensions, width × height × thickness (in mm)	Measuring time (h)	Background/signal† (%)	MSC‡ (%)
[0 0 1]	ΓA	7.95 × 7.95 × 1.13	20.5	13.2	13.3
[1 0 0]	ΓM	8.18 × 8.09 × 1.31	31.0	11.1	14.5
[1 1 0]	ΓK	8.02 × 8.12 × 1.15	32.0	10.2	13.6
[1 0 1]	ΓL	8.12 × 8.03 × 1.16	28.5	14.9	13.6
[2 2 3]	ΓH	8.06 × 8.00 × 1.04	31.5	12.2	12.8

† Background to signal ratio under the CP.   ‡ Ratio of multiple to single scattering under the CP.

$$n(\mathbf{p}) = \frac{1}{2\pi^3} \sum_j \left| \int \psi_j(\mathbf{r}) \exp\left(-i\,\mathbf{p}\cdot\mathbf{r}\right) \mathrm{d}^3\mathbf{r} \right|^2. \qquad (2)$$

Subtraction of two directional CPs, measured at two specific crystallographic directions, removes all isotropic components from the CPs (*i.e.* core electrons and background contributions) and forms the so-called difference profiles (anisotropies), which reveal the anisotropy of the electron momentum density distribution associated with the crystal symmetry and the shape of the Fermi surface (fermiology) of the studied material (Sakurai *et al.*, 1995; Hämäläinen *et al.*, 1996; Dugdale *et al.*, 2000; Reniewicz *et al.*, 2001; Mizusaki *et al.*, 2003; Bellin *et al.*, 2004; Dugdale *et al.*, 2006; Brancewicz *et al.*, 2007; Huotari *et al.*, 2007; Choudhary *et al.*, 2011; Brancewicz *et al.*, 2013; Sharma *et al.*, 2015).

A medium-resolution (0.42 a.u.; 1 a.u. of momentum = 1.9929×10^{-24} kg m s^{-1}) Compton scattering experiment on a Zn single crystal was performed for the first time at the Institute of Experimental Physics, University of Białystok, on the high-energy Compton spectrometer with the use of 662 keV γ radiation from a ^{137}Cs isotope source (Reniewicz *et al.*, 2001). CPs were measured along four high-symmetry directions (ΓA, ΓM, ΓK and close to ΓH). Despite the long-term measurements of one CP (300–600 h), the relatively low statistics of the anisotropy profiles and the low achieved resolution were not sufficient to observe the subtle features of the electron momentum density anisotropy in Zn near the Fermi momentum. Although statistically significant differences were observed between the experimental data and Korringa–Kohn–Rostoker (KKR) calculations, especially below the Fermi momentum, they were not sufficiently well shaped for making a rigorous comparison of the experimental data and theory. It was thus obvious that high-resolution Compton experiments have to be carried out to provide reliable tests of first-principles calculations.

High-resolution (0.16 a.u.) CPs of hexagonal Zn have already been measured with the use of 57 keV synchrotron radiation along the ΓA, ΓK and ΓH directions at the ESRF on beamline ID15B (Bellin *et al.*, 2004). The results obtained exhibited a rather low statistical value and showed evident discrepancies between experiment and KKR calculations, especially in the low momentum region, where the sharp fermiology features predicted by KKR calculations should be observed. Therefore, either the experiment was inconclusive or the theory did not deliver proper results. This called for a

new experiment with improved momentum resolution and better statistical accuracy, and also other calculations based on a different theoretical technique than KKR.

Following this idea, the need for high-resolution and high experimental statistics Compton scattering measurements for hexagonal metals (Mg, Zn, Cd) with the use of synchrotron radiation was suggested by Brancewicz *et al.* (2007). This kind of experiment was successfully carried out for a magnesium single crystal with the lowest atomic number among those three metals (Brancewicz *et al.*, 2013). The good quality of the four measured directional CPs allowed for a quantitative discussion of data agreement with theoretical calculations, even in the region of low electron momenta, and successful reconstruction of the 3D electron momentum density using the maximum entropy method (MEM).

In this paper we present our results of directional CP measurements with high resolution and high experimental statistics for the next of the three metals mentioned above – a Zn single crystal. The work has four main goals:

(i) Comparison of the results of similar (but not identical) measurements made on synchrotrons at two locations with the use of different synchrotron radiation energies [57 keV at ESRF (Bellin *et al.*, 2004) and 115.6 keV at SPring-8 (current data)] and using different procedures for experimental data analysis. In order to improve the statistics we decided to use samples over 1 mm thick (Table 1). This results in an increase in the contribution of unwanted photon multiple scattering in the sample. The correction for this effect must be simulated numerically and then subtracted from the analysed CP.

(ii) Therefore in this study the new *MUSCAT* program has been used for the multiple-scattering simulations. It was written to deal with different experimental geometries and proved its excellent accuracy in a series of test experiments carried out on the BL08W station at SPring-8 (Brancewicz *et al.*, 2016). Nonetheless, another check of the procedure is recommended and here, in a real experiment, we did this test again.

(iii) The third task was to provide another calculation of the electronic bands and corresponding Compton profiles, and see how the *ab initio* theoretical results may differ from the KKR ones used so far. Another publication (Bross, 2005) shows that the KKR approach gives somewhat higher CPs than observed. In this situation the *Wien2k* code (Blaha *et al.*, 2001) gave a hope of improving results. As is known, KKR uses a semi-relativistic approach (relativistic core and non-relativistic

valence electrons). In the *Wien2k* code the calculations are fully relativistic. Comparison of Mg with Zn or Cd shows that this may be important in the case of Zn or Cd because the relativistic states of the core may influence the higher-lying energy states. These states are of interest because they contribute quite a bit to the shape of the Compton profile. In addition, to describe the electronic correlations and improve the local density approximation (LDA), the Lam–Platzman correction (Lam & Platzman, 1974) was used in the calculations so far. In our new calculations, the exchange-correlation potential in the form proposed by Perdew, Burke and Erzenhof (Perdew *et al.*, 1996) has been used. This potential takes into account the electron-density gradient, which may be important for getting a good description of the electronic states. Moreover, the Lam–Platzman correction was no longer necessary. A fuller description of the theoretical issues is given in the *Theory* section.

(iv) Finally, we want to check whether the expected discrepancies between theories and experiment can bring some important conclusions.

In order to better understand the origin of the differences, a full 3D reconstruction of the electron momentum density distribution in a Zn single crystal should be very helpful. This is, however, not an easy task when the anisotropies are small, especially when the MEM (our favourite) is used for such a reconstruction. Our first results showed that a reliable reconstruction requires a lot of care and it would be too early to present a preliminary reconstruction. We thus leave the reconstruction to a subsequent paper.

2. Experiment

Similar to our earlier studies (Reniewicz *et al.*, 2001; Bellin *et al.*, 2004), we had the opportunity to measure the directional CPs of Zn, but along seven crystallographic directions in reciprocal space. Here we present the CPs and their anisotropies measured along five high-symmetry directions in the first Brillouin zone: ΓA, ΓM, ΓK, ΓH and ΓL (Fig. 1). In the future an additional two CPs, unrelated to the high-symmetry directions in the first Brillouin zone (BZ), will be used to improve the accuracy of the 3D electron momentum density reconstruction in Zn.

All samples were cut from a zinc crystal ingot grown by the Bridgeman method at the Institute of Nuclear Studies in
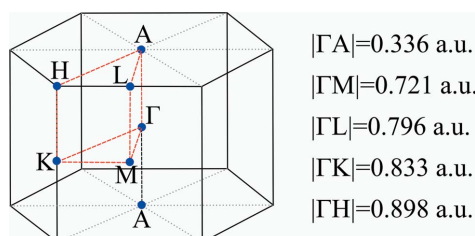
Świerk, Poland. A standard procedure of polishing and etching was applied to all samples in order to assign their orientation using the X-ray Laue technique. The parameters of all samples, together with the indexing of directions in the hexagonal structure and the main experimental details, are given in Table 1.

Compton scattering measurements were performed using a Cauchois-type X-ray spectrometer on the BL08W beamline at SPring-8 (Sakurai & Itou, 2004; Hiraoka *et al.*, 2001; Itou & Sakurai, 2004; Itou *et al.*, 2001). Incident X-rays emitted from a multipole wiggler were monochromated to 115.6 keV by a bent-type Si (400) crystal. The size of the incident X-ray beam was 2.5 mm in height and 5 mm in width at the sample position. Measurements were performed under vacuum and room-temperature conditions. The scattering angle was fixed at 165°. The Compton-scattered X-rays were measured by a 2D position-sensitive detector (PSD) and registered on a charge-coupled device (CCD) matrix of size 1344 × 1024 pixels. The momentum ranges of the CPs selected for analysis span from −10 a.u. to 10 a.u., covering an energy range of 70–90 keV in the scattered spectrum. Two sets of measurements were made for all samples. Each time the samples in the goniometer were changed, the repeatability of the measurements was also tested to eliminate any systematic errors (imprecise positioning of the sample, its disorientation *etc.*).

In order to get the CPs, the measured spectra were corrected for background scattering, absorption of photons in the sample, detector efficiencies, scattering cross section and multiple-scattering contribution (MSC) (Brancewicz *et al.*, 2013). The spectrum of multiple-scattered X-rays was simulated by the Monte Carlo method with the use of the *MUSCAT* program (Brancewicz *et al.*, 2016), which takes into account the exact experimental geometry [up to triple scattering in the sample (Fig. 2)] and subtracts it from the measured total spectrum. The MSC correction significantly
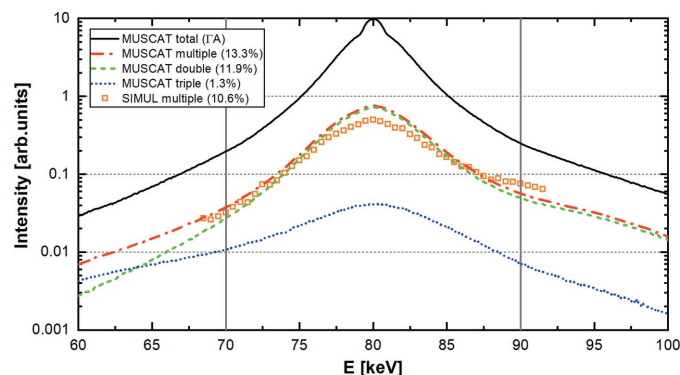

Figure 1
The first Brillouin zone for the hcp structure, marked with high-symmetry points (blue dots) that define the five directions in reciprocal space chosen for the CP measurements. An irreducible 1/24th part (wedge) of the zone is marked by red dashed lines. All major lengths are given on the right-hand side of the figure.

|ΓA|=0.336 a.u.
|ΓM|=0.721 a.u.
|ΓL|=0.796 a.u.
|ΓK|=0.833 a.u.
|ΓH|=0.898 a.u.

Figure 2
Example of a simulated spectrum of Compton scattered X-rays by the *MUSCAT* program. The black solid line represents the total spectrum, the green dashed line is a spectrum of double-scattered photons, the blue dotted line is a spectrum of triple-scattered photons and the red dashed–dotted line is the total spectrum of multiple-scattered photons in the sample (here, double- plus triple-scattered contributions). The multiple (double + triple) scattering simulation result obtained with the use of an older procedure (*SIMUL*) is shown for comparison using orange empty squares. The range 70–90 keV (grey vertical lines) is approximately equal to the momentum range from −10 a.u. to 10 a.u.

affects the final CP. Its shape especially affects the CP symmetry, while the intensity of the subtracted MSC spectrum affects the profile height. It can be seen that the new approach (*MUSCAT*) changes the shape of the MSC correction in a significant way compared with the results obtained with the use of the older procedure (*SIMUL*; Sakai, 1987).

The overall momentum resolution in the present measurements turned out to be 0.12 a.u., which is the typical resolution of Compton scattering experiments on BL08W. The areas under the final CPs, in the range 0–10 a.u., were normalized to 13.673 electrons of the Zn atom involved in the Compton scattering in this momentum range, calculated on the basis of the theoretical KKR CPs.

After applying all the aforementioned corrections, high-quality directional CPs were obtained, also satisfying the so-called consistency condition (Kontrym-Sznajd & Samsel-Czekała, 2000).

3. Theory

Band-structure calculations for Zn are certainly more difficult than the previously studied Mg (Brancewicz *et al.*, 2013). The main goal of those procedures was to find the wavefunctions of all electrons. The base of orbital functions (as for a single atom) was the core area, while in the interstitial area they were expanded into plane waves and stitched at the border. For Mg, this is a very good expansion, because its valence electrons are almost free. There was also no problem with splitting the wavefunctions into ones describing core electrons (these are closed in atomic spheres) and ones describing delocalized electrons. Things always get complicated when $3d$ electrons are present like in Zn; here, the states $1s$, $2s$ and $2p$ (real core) are very deep, whereas the states $3s$, $3p$, and especially $3d$, are not. In addition, $3d$ as a narrow band is poorly linearized (this applies to almost all d-electron atoms). As a result, there is something similar to the core (often called semi-core) and valence states.

3.1. KKR

The first electronic band-structure and momentum density calculations of hexagonal Zn were based on the KKR Green's function method, utilizing the muffin-tin approximation to the crystal potential (Reniewicz *et al.*, 2001). All electrons were included and the von Barth–Hedin local density approximation (LDA) (Von Barth & Hedin, 1972) to the exchange-correlation potential was used. The band-structure problem was solved to a high degree of self-consistency (energy bands, Fermi energy and potentials converged to better than 1 meV) using $l_{max} = 3$ (maximum angular momentum cut-off). In order to find the CPs, the momentum density $n(\mathbf{p})$ was calculated on a mesh containing $24 \times 3153 \times 2799$ p points [see details in the work of Kaprzyk (1997)]. The 2D integrations involved in the evaluation of the CPs were carried out using the tetrahedral method of Lehmann & Taut (1972). The final CPs were computed along the ΓA, ΓM, ΓK, ΓL and ΓH directions on a 201-point uniformly spaced mesh in q (momentum transfer)

over the range 0–15 a.u. The Lam–Platzman correction was calculated in the final stage in a standard way using all the electrons, as required by the LDA method.

3.2. Density functional theory (DFT)

The new electronic structure calculations presented in this paper use the *ab initio* full potential linearized augmented plane-wave method with local orbitals (FP-LAPW+lo), as implemented in the *Wien2k* code. In contrast to the former KKR calculations, where the LDA was made, in this case the generalized gradient approximation (GGA) with revised exchange-correlation potential (Perdew *et al.*, 1996) was adapted. To solve the single-electron Kohn–Sham equation, the wavefunction was expanded into lattice harmonics (inside a muffin-tin of radius R_{MT} = 2.5 a.u.) and plane waves (in the interstitial region). The number of plane waves was defined by the maximum momentum K_{max} = 3.2 a.u.$^{-1}$ (equivalent to $R_{MT}K_{max}$ = 8), which is a reasonable value for this type of material. In order to reduce the discontinuity of the wavefunction at the border of the muffin-tin, spherical harmonics up to $(l_{max}; m_{max}) = (6; 6)$ were used [for the space group $P6_3/mmc$, the allowed spherical harmonics are (0; 0), (2; 0), (3; 3), (4; 0), (5; 3), (6; 0) and (6; 6)]. The chosen energy threshold to separate core and valence states was $E_{th} = -10$ Ry, which corresponds to the $1s$, $2s$ and $2p$ atomic states (treated as unperturbed and fully relativistic). This choice allows one to avoid so-called charge leaking from the sphere. Integrations inside the BZ were made using a grid of 2496 k points in the irreducible wedge (Fig. 1), which is equivalent to probing $47 \times 47 \times 22$ for a full first BZ. Convergence criteria were chosen as follows: 10^{-6} Ry for the total energy difference and 10^{-4} e for the charge density. Since the *Wien2k* code has no subroutines for momentum density and CP calculations, some extra effort was needed.

The momentum density was calculated as:

$$n(\mathbf{p}) = \frac{\Omega_0}{(2\pi)^2} \sum_n \sum_{\mathbf{k}}^{BZ} \theta\left(\epsilon_F - \epsilon_{n,\mathbf{k}}\right) \sum_{\mathbf{K}} \delta_{\mathbf{k},\mathbf{p}-\mathbf{K}} \left|a_{n,\mathbf{k}}^{PW}(\mathbf{K})\right|^2, \quad (3)$$

where $a_{n,\mathbf{k}}^{PW}(\mathbf{K})$ is the plane-wave coefficient of state (n, $\mathbf{k}$) corresponding to the reciprocal vector $\mathbf{K}$ (Pylak *et al.*, 2013). Here, 1000 k points inside an irreducible wedge of the BZ were used, together with 6139 reciprocal $\mathbf{K}$ vectors, to find the momentum density. Directional CPs were calculated along the five high-symmetry directions in the first BZ (ΓA, ΓM, ΓK, ΓL and ΓH) by the 2D Simpson numerical integration of

$$J(q, \hat{e}) = \int_0^P \int_0^{2\pi} p \, dp \, d\phi \, n(\mathbf{p}) \, \delta(\mathbf{p}\hat{e} - q), \quad (4)$$

where $\hat{e}$ defines the direction of CP. The upper limit of the integration was $P = 25$ a.u.$^{-1}$.

The core electrons are treated fully relativistically in our new DFT calculations, *i.e.* the Dirac–Slater equation is solved. For valence electrons and spin–orbit coupling the scalar-relativistic approach (equivalent of semi-relativistic) was used. The spin–orbit coupling that is in the Dirac equation can significantly affect the shapes and positions of the energy
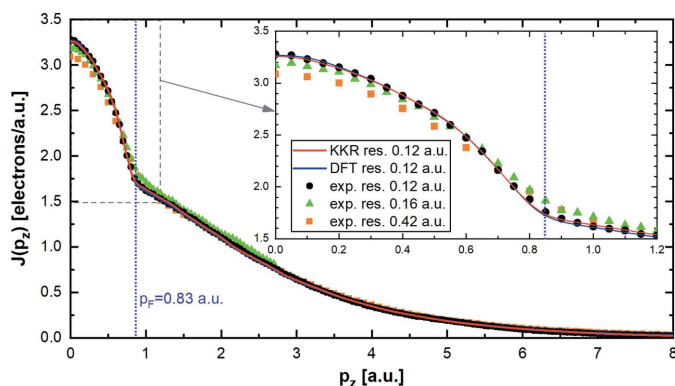
bands. In Mg, where such effects are negligible, the relativistic corrections are very small. Zn already requires the aforementioned scalar-relativistic approach. It seems that relativistic approximations most strongly affect the deep states of the $3d$ valence electrons, which deform the states around the Fermi energy level and can affect the shape of the CP.

4. Results, discussion and conclusions

As an example, the ΓA CP of the Zn valence electrons (after subtracting the contribution of the core electrons from the total profile) is presented in Fig. 3. The areas under the final valence profiles in the range 0–10 a.u. were normalized to 5.783 electrons (13.673 electrons under the total CPs, 7.890 core electrons), calculated on the basis of the theoretical KKR CPs. The other four profiles are all very similar in shape. The differences between them are visible only in anisotropies (*i.e.* as the differences between two corresponding profiles).

Two components are clearly visible in the shape of the valence CPs of Zn. The first one (narrow) has a parabolic shape and is located below the Fermi momentum. The second one is very wide and extends to higher momenta. It is mainly the $4s^2$ electrons that are responsible for the narrow component of the CP and the $3d^{10}$ electrons for the wide one. Fig. 3 shows the sum of both profiles, where the $4s^2$ profile is located on top of the $3d^{10}$ profile, the range of which also starts at 0 a.u. The parabolic shape of the $4s^2$ profile clearly demonstrates the free character of its electrons, and is very similar to the valence profile of hexagonal magnesium formed by $3s^2$ electrons (Brancewicz *et al.*, 2006).

To test the quality and goodness of the experimental profiles, their differences with respect to the proper theoretical profiles are usually presented. As an alternative example, here
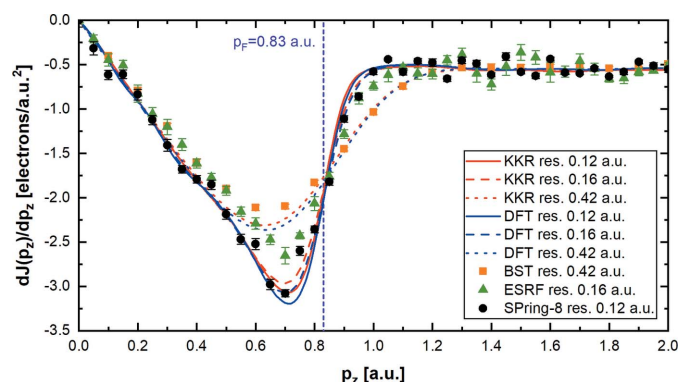
we show in Fig. 4 the first derivative of the directionally weighted average profile, which enhances the monotonicity of CP at low momenta. The weights are the multiplicity of appropriate directions in the first BZ (one for direction ΓA, three for ΓM and ΓK, and six for ΓH and ΓL) and the experimental uncertainty was calculated as an average deviation from the weighted average at each point. The two earlier measurements with moderate (0.42 a.u.; Reniewicz *et al.*, 2001) and high (0.16 a.u.; Bellin *et al.*, 2004) resolution are shown for comparison. It is possible to determine the Fermi momentum on the basis of the location of the sharp edge in the derivatives, which for all the relationships shown is equal to about 0.83 a.u. One may note that the theory delivers results that agree with the experimental data collected at medium (0.42 a.u.) and high (0.12 a.u.) resolution, while the data measured at the ESRF (green triangles, resolution 0.16 a.u.) apparently disagree with both the KKR and DFT calculations. Thus, we suspect that the data collected at the ESRF, because of the limited range of the measured electron momentum and poor statistics, can not be trusted. On the other hand, the data collected with 0.12 a.u. are richer than those collected with 0.42 a.u. In fact, this was our target. On the theoretical side, the first derivatives of the directionally averaged theoretical KKR and DFT profiles of the same resolution display very similar shapes.

Since the anisotropies of the CPs in a single crystal of Zn are small (see below), it is possible to use the directionally weighted average profile from the available CPs (both theoretical and experimental) to calculate the isotropic electron momentum density $n(p)$ without any essential loss of physical information:

$$n(p) = -\frac{1}{2\pi p_z} \frac{\mathrm{d}J(p_z)}{\mathrm{d}p_z}\bigg|_{p=p_z}. \tag{5}$$

Figure 3
High-resolution (0.12 a.u.) CP of valence electrons in Zn measured along the ΓA direction (black circles), together with the corresponding theoretical KKR (red solid line) and DFT (blue solid line) calculations convoluted with a Gaussian of FWHM = 0.12 a.u. to mimic the resolution of the experimental data. Our previous data are plotted for comparison: orange squares, medium resolution 0.42 a.u. (Reniewicz *et al.*, 2001), and green triangles, high resolution 0.16 a.u. (Bellin *et al.*, 2004). The vertical blue dotted line shows the expected location of the Fermi momentum in Zn ($p_F = 0.83$ a.u. as calculated within the framework of the free-electron model). All experimental uncertainties are smaller than the size of the points. The inset shows a closer look at the behaviour of the CPs in the vicinity of the Fermi momentum.

Figure 4
The first derivatives of the experimental and theoretical directionally weighted average valence CPs of zinc are shown for three experiments at different resolutions: 0.12 a.u. (current data from SPring-8, black circles), 0.16 a.u. [experiment at ESRF (Bellin *et al.*, 2004), green triangles] and 0.42 a.u. [our experiment with the use of an isotope source (Reniewicz *et al.*, 2001), orange squares]. Derivatives of the theoretical KKR (red lines) and DFT (blue lines) profiles are also shown at three different resolutions: 0.12 a.u. (solid lines), 0.16 a.u. (dashed lines) and 0.42 a.u. (dotted lines).
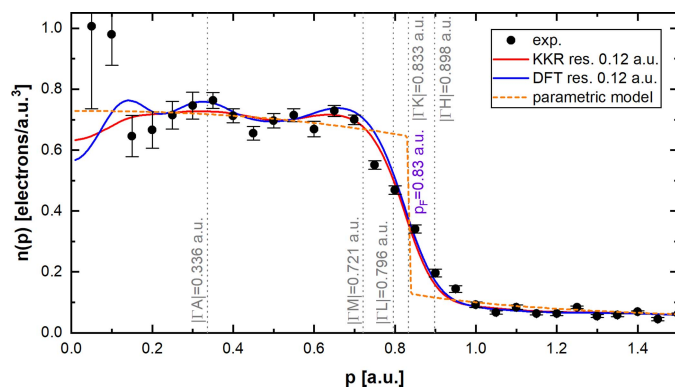
The electron momentum density can be also modelled with the use of the modified Schülke parametric function [equation (10) in the work of Brancewicz *et al.* (2013)], which covers the density of free $4s^2$ electrons with an additional Gaussian function to fit the $3d^{10}$ electron density. The parameters were chosen to get the best fit of the average experimental CP (resolution of 0.12 a.u.) and calculated from the electron density using the equation

$$J(p_z) = 2\pi \int_{p_z}^{\infty} p\, n(p)\, \mathrm{d}p. \qquad (6)$$

The results of the above calculations and fitting are shown in Fig. 5.

The isotropic momentum densities calculated from equation (5) based on the averaged theoretical KKR and DFT CPs are quite similar in shape in the region above 0.5 a.u. Both densities show a similar drop near the Fermi momentum (0.83 a.u.), coinciding with the |ΓK| length. The maxima of $n(p)$ are visible around 0.72 a.u. (|ΓM| length). However the $n_{\mathrm{DFT}}(p)$ calculated from the DFT CPs shows two more maxima at around 0.34 a.u. (|ΓA| length) and 0.15 a.u. (not connected to any specific direction), and two minima at around 0.25 a.u. and 0.5 a.u. (also not connected to any specific direction in the first BZ). It seems that, except for the lowest momenta, this oscillating character of the theoretical $n_{\mathrm{DFT}}(p)$ below the Fermi momentum is confirmed by the density calculated from the corresponding experimental data. The sharp upward jump of the experimental electron momentum density in the range below 0.1 a.u has very low precision and cannot be determined to be real.

The parametric model of $n(p)$, fitted to the directionally averaged Compton experimental profile via equation (6) (represented by the orange dashed line in Fig. 5), shows that in the directionally averaged momentum density in Zn an elec-

tron-density jump of about 0.5 e a.u.$^{-3}$ should exist at the Fermi momentum, which may be evidence of a lack of (or small) $3d^{10}$–$4s^2$ electron correlations. The same behaviour is not visible in the isotropic momentum density distribution calculated from the experimental data using equation (5) because of the limited resolution (0.12 a.u.) and the large steps on the momentum axis (0.05 a.u.) used to display the data. The parametric model can be used as the 'prior' to reconstruct the 3D electron momentum density in Zn.
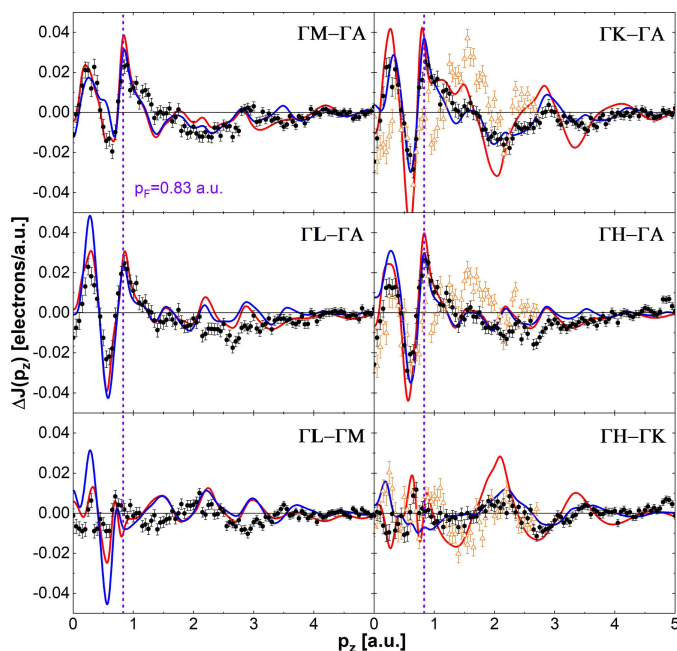
As already mentioned, the most commonly used and effective method of comparing theoretical CPs with experimental ones is to demonstrate their anisotropy. Subtraction of profiles measured in two specific crystallographic directions removes the isotropic contribution from the core electrons as well as other (often unknown) isotropic contributions, together with any possible systematic experimental uncertainties. In this way one obtains the so-called differential profile, which shows the anisotropy of the electron momentum density in the tested material and provides valuable information on the behaviour of the valence electrons responsible for the creation of solids and their properties.

Anisotropies were calculated for conventional right-sided profiles (for $p_z > 0$) as well as for averaged (left- and right-sided) profiles. Both methods offered the same result within the experimental uncertainty of one standard deviation, so the averaged profiles bearing smaller uncertainties are presented in what follows.

The main anisotropies of the measured directional CPs are presented in Fig. 6, together with the corresponding KKR and DFT theoretical ones convoluted to a resolution of 0.12 a.u. Our previous data (Bellin *et al.*, 2004) of slightly worse resolution (0.16 a.u.) are also shown, to compare the shape of the anisotropy and the quality of the newly measured data.

The maximum amplitude of the CP anisotropies of hexagonal Zn (seen in Fig. 6 in the high-resolution experiment) is less than 0.7% of $J(0)$, which is much smaller than that measured for high-symmetry cubic systems (*e.g.* Bansil *et al.*, 1998). The directional difference profiles (anisotropies) of the CPs show general agreement with both theoretical KKR and DFT calculations convoluted to the experimental resolution (Fig. 6), although depending on the direction sometimes the KKR or DFT calculations seem to describe the data better. The amplitudes and zero-crossing positions of the experimental anisotropies agree well with the calculated ones. However, within the limits of experimental accuracy, it cannot be determined which theory describes the experimental data better below p_F. As in the case of the averaged profiles, the anisotropies for the data collected at the ESRF (orange empty triangles in Fig. 6) apparently disagree with the theory. This shows how important it was to make independent experiments at SPring-8.

At momenta above 1 a.u. the anisotropies calculated by the KKR and APW methods are similar concerning zero-crossing, but the KKR data show bigger amplitudes than the DFT calculations, especially for anisotropies with the ΓK profile. Moreover, there is a significant disagreement between the two theories in the case of ΓH–ΓK anisotropy at practically all

Figure 5
The averaged momentum density of valence electrons $n(p)$ in Zn, calculated from equation (5). Grey dotted vertical lines show the major lengths in the first BZ (see Fig. 1) and the Fermi momentum p_F. The experimental data are represented by solid black circles, and the theoretical KKR and DFT data are shown by solid red and blue lines, respectively. Both theoretical profiles were convoluted with a Gaussian of FWHM = 0.12 a.u. to mimic the resolution of the experimental data. The orange dashed line shows the modelled momentum density distribution as given by Brancewicz *et al.* (2013), which leads [through equation (6)] to the best description of measured CPs.

Figure 6
High-resolution (0.12 a.u.) experimental CP anisotropies in Zn (black solid circles), together with the corresponding KKR (red lines) and DFT (blue lines) theoretical profile calculations convoluted with a Gaussian of FWHM = 0.12 a.u. to mimic the resolution of the present experiment. In addition, our previous high-resolution (0.16 a.u.) experimental data (Bellin *et al.*, 2004) are shown by orange empty triangles in three of the panels. The Fermi momentum is marked by the vertical blue dashed lines.

momenta. For this anisotropy DFT predicts much lower amplitudes and completely different behaviour in the range 0–1.5 a.u.

Sharp features predicted by both theories in the momentum region below 1 a.u. are quite well observed experimentally in most cases, which contrasts with previous measurements (Reniewicz *et al.*, 2001; Bellin *et al.*, 2004). In the case of small anisotropies, as for the differential profiles ΓL–ΓM and ΓH–ΓK, agreement between the experiment and both theories in this momentum region is no longer as acceptable. Within the experimental uncertainty the KKR theory seems to be in better agreement with the experiment in terms of both amplitude (ΓL–ΓM anisotropy) and the location of the minimum and maximum (ΓH–ΓK anisotropy).

Above the Fermi momentum, better agreement of the experiment with DFT is observed in all cases. In particular, where the amplitudes of the theoretical anisotropies differ significantly (ΓK–ΓA and ΓH–ΓK), the experimental points clearly follow the DFT. Some small discrepancies between the experimental and theoretical anisotropies are still observed in the range from around 1.5 to around 3.0 a.u. This may be due to some unknown experimental artefacts that were not taken into account during the data-processing procedure.

5. Summary

High-resolution CPs of a hexagonal Zn single crystal have been measured along five high-symmetry directions in reci-

procal space with the use of 115.6 keV synchrotron radiation on the BL08W station at SPring-8. The experimental data were compared with the corresponding theoretical KKR and DFT calculations and our previous experiments of medium (0.42 a.u.) and high (0.16 a.u.) resolution data. This time the quality of the measured high-resolution CPs was much better, because the profiles were measured over a wide range of momentum up to 10 a.u. (previously to 2.7 a.u.), with significantly better experimental statistics, as seen in Fig. 6. This allows us to observe small fluctuations in electron density in the first Brillouin zone (Fig. 5) and at higher electron momenta (Fig. 6). We believe that such high-quality data can be successfully used for future 3D electron momentum density reconstruction.

An experiment with better energy resolution (115.6 keV at SPring-8) than that reached at the ESRF (57 keV) has been carried out and proved to deliver more reliable data. This new experiment also covered a much broader electron momentum range (10 a.u. versus 2.7 a.u., respectively; see Fig. 3). In addition, more directions were measured.

The new *MUSCAT* program confirmed its usefulness in simulations of multiple scattering of photons when different sample geometries in the beam were considered. The simulated MSC level from 12.8% to 14.5% for samples of different thicknesses (Table 1) was more than 3% higher than that obtained using older procedures (Fig. 2), appropriate only for the approximate cylindrical geometry of the experiment (values from 9.6% to 11.1%). The accuracy of this type of simulation is on the level of about 1%.

Finally, it seems that recent theoretical calculations using DFT describe the experimental results better than KKR, especially above the Fermi momentum. In the lower momentum region both theories reproduce the experimental data to a comparable level of accuracy, albeit still showing some statistically significant disagreements. Inconsistencies in theoretical low-momentum profiles are usually interpreted as a result of incomplete treatment of electron correlation, although both presented theories take this effect into account through the LDA+Lp (KKR) and the newer GGA (DFT) exchange-correlation potential approximations. We are still sure that the correlation effects are not precisely taken into account during theoretical band-structure calculations. Maybe using an even newer approximation like meta-GGA (Tao *et al.*, 2003) could produce better results.

In spite of the high resolution attained in the experiment, some differences remain between experiment and theory, the origin of which is presently not well understood. We believe that the 3D reconstruction of the electron momentum distribution can show which parts of the momentum space may be responsible for such a situation. Whether the differences depicted in Fig. 6 are due to experimental or theoretical reasons remains to be resolved.

References

Almond, D. P., Lea, M. J. & Dobbs, E. R. (1975). *Proc. R. Soc. London Ser. A*, **343**, 537–560.

Bansil, A., Kaprzyk, S., Andrejczuk, A., Dobrzyński, L., Kwiatkowska, J., Maniawski, F. & Żukowski, E. (1998). *Phys. Rev. B*, **57**, 314–323.

Barth, U. & Hedin, L. (1972). *J. Phys. C: Solid State Phys.* **5**, 1629–1642.

Bellin, Ch., Honkimäki, V., Reniewicz, H., Zaleski, P., Andrejczuk, A., Dobrzyński, L., Żukowski, E. & Kaprzyk, S. (2004). *J. Alloys Compd.* **362**, 314–317.

Blaha, P., Schwarz, K., Madsen, G. K. H., Kvasnicka, D. & Luitz, J. (2001). *Wien2k, An Augmented Plane Wave and Local Orbitals Program for Calculating Crystal Properties*. Technische Universität Wien, Austria.

Borghese, F. & Denti, P. (1971). *Nuov. Cim. B*, **3**, 34–44.

Borghese, F. & Denti, P. (1974). *Nuov. Cim. B*, **20**, 236–246.

Brancewicz, M., Andrejczuk, A., Dobrzyński, L., Reniewicz, H. & Żukowski, E. (2007). *Nucl. Instrum. Methods Phys. Res. B*, **255**, 395–398.

Brancewicz, M., Itou, M. & Sakurai, Y. (2016). *J. Synchrotron Rad.* **23**, 244–252.

Brancewicz, M., Pylak, M., Andrejczuk, A., Żukowski, E., Dobrzyński, L., Sakurai, Y., Itou, M. & Sormann, H. (2013). *J. Phys. Soc. Jpn*, **82**, 074702.

Brancewicz, M., Reniewicz, H., Andrejczuk, A., Dobrzyński, L., Żukowski, E. & Kaprzyk, S. (2006). *Solid State Phenom.* **112**, 123–132.

Bross, H. (2005). *Phys. Rev. B*, **72**, 115109.

Choudhary, G., Raykar, V., Tiwari, S., Dashora, A. & Ahuja, B. L. (2011). *Phys. Status Solidi B*, **248**, 212–219.

Cooper, M. J., Mijnarends, P. E., Shiotani, N., Sakai, N. & Bansil, A. (2004). *X-ray Compton Scattering.* Oxford University Press.

Daniuk, S., Jarlborg, T., Kontrym-Sznajd, G., Majsnerowski, J. & Stachowiak, H. (1989). *J. Phys. Condens. Matter*, **1**, 8397–8406.

Dugdale, S. B., Fretwell, H. M., Chen, K. J., Tanaka, Y., Shukla, A., Buslaps, T., Bellin, Ch., Loupias, G., Alam, M. A., Manuel, A. A., Suortti, P. & Shiotani, N. (2000). *J. Phys. Chem. Solids*, **61**, 361–363.

Dugdale, S. B., Watts, R. J., Laverock, J., Major, Zs., Alam, M. A., Samsel-Czekała, M., Kontrym-Sznajd, G., Sakurai, Y., Itou, M. & Fort, D. (2006). *Phys. Rev. Lett.* **96**, 046406.

Hämäläinen, K., Manninen, S., Kao, C.-C., Caliebe, W., Hastings, J. B., Bansil, A., Kaprzyk, S. & Platzman, P. M. (1996). *Phys. Rev. B*, **54**, 5453–5459.

Harrison, W. A. (1962). *Phys. Rev.* **126**, 497–505.

Hiraoka, N., Itou, M., Ohata, T., Mizumaki, M., Sakurai, Y. & Sakai, N. (2001). *J. Synchrotron Rad.* **8**, 26–32.

Huotari, S., Sternemann, C., Volmer, M., Soininen, J. A., Monaco, G. & Schülke, W. (2007). *Phys. Rev. B*, **76**, 235106.

Itou, M., Hiraoka, N., Ohata, T., Mizumaki, M., Deb, A., Sakurai, Y. & Sakai, N. (2001). *Nucl. Instrum. Methods Phys. Res. A*, **467–468**, 1109–1112.

Itou, M. & Sakurai, Y. (2004). *AIP Conf. Proc.* **705**, 901–904.

Joseph, A. S. & Gordon, W. L. (1962). *Phys. Rev.* **126**, 2, 489–497.

Kaprzyk, S. (1997). *Acta Phys. Pol. A*, **91**, 135–150.

Kontrym-Sznajd, G. & Samsel-Czekała, M. (2000). *Appl. Phys. Mater. Sci. Process.* **70**, 89–92.

Lam, L. & Platzman, P. M. (1974). *Phys. Rev. B*, **9**, 5122.

Lehmann, G. & Taut, M. (1972). *Phys. Status Solidi B*, **54**, 469–477.

Mizusaki, S., Hiraoka, N., Yamamoto, I., Itou, M., Sakurai, Y. & Yamaguchi, M. (2003). *J. Phys. Soc. Jpn*, **72**, 1145–1151.

Novikov, D. L., Katsnelson, M. I., Trefilov, A. V., Freeman, A. J., Christensen, N. E., Svane, A. & Rodriguez, C. O. (1999). *Phys. Rev. B*, **59**, 4557–4560.

Perdew, J. P., Burke, K. & Ernzerhof, M. (1996). *Phys. Rev. Lett.* **77**, 3865–3868.

Perkkiö, S., Sharma, B. K., Manninen, S., Paakkari, T. & Ahuja, B. L. (1991). *Phys. Status Solidi B*, **168**, 657–664.

Pylak, M., Dobrzyński, L. & Sormann, H. (2013). *Phys. Scr.* **88**, 035708.

Reniewicz, H., Andrejczuk, A., Dobrzyński, L., Żukowski, E. & Kaprzyk, S. (2001). *J. Phys. Condens. Matter*, **13**, 11597–11606.

Sakai, N. (1987). *J. Phys. Soc. Jpn*, **56**, 2477–2485.

Sakurai, Y. & Itou, M. (2004). *J. Phys. Chem. Solids*, **65**, 2061–2064.

Sakurai, Y., Tanaka, Y., Bansil, A., Kaprzyk, S., Stewart, A. T., Nagashima, Y., Hyodo, T., Nanao, S., Kawata, H. & Shiotani, N. (1995). *Phys. Rev. Lett.* **74**, 2252–2255.

Sharma, K., Sahariya, J. & Ahuja, B. L. (2015). *J. Alloys Compd.* **645**, 414–420.

Stark, R. W. & Falicov, L. M. (1967). *Phys. Rev. Lett.* **19**, 795–798.

Steenhaut, O. L. & Goodrich, R. G. (1970). *Phys. Rev. B*, **1**, 4511–4520.

Tao, J., Perdew, J. P., Staroverov, V. N. & Scuseria, G. E. (2003). *Phys. Rev. Lett.* **91**, 146401.